J Physiol 588.3 (2010) pp 495–510

The mechanism of the resistance to stretch of isometrically contracting single muscle fibres

Luca Fusi[1], Massimo Reconditi[1,2], Marco Linari[1,2], Elisabetta Brunello[1], Ravikrishnan Elangovan[1], Vincenzo Lombardi[1] and Gabriella Piazzesi[1]

[1]*Laboratory of Physiology, Department of Evolutionary Biology, University of Florence, Via G. Sansone 1, 50019 Sesto Fiorentino (FI), Italy*
[2]*Consorzio Nazionale Interuniversitario per le Scienze Fisiche della Materia, Florence, Italy*

Rapid attachment to actin of the detached motor domain of myosin dimers with one motor domain already attached has been hypothesized to explain the stretch-induced changes in X-ray interference and stiffness of active muscle. Here, using half-sarcomere mechanics in single frog muscle fibres (2.15 μm sarcomere length and 4°C), we show that: (1) an increase in stiffness of the half-sarcomere under stretch is specific to isometric contraction and does not occur in rigor, indicating that the mechanism of stiffness increase is an increase in the number of attached motors; (2) 2 ms after 100 μs stretches (amplitude 2–8 nm per half-sarcomere) imposed during an isometric tetanus, the stiffness of the array of myosin motors in each half-sarcomere (e_m) increases above the isometric value (e_{m0}); (3) e_m has a sigmoidal dependence on the distortion of the motor domains (Δz) attached in isometric contraction, with a maximum ~2 e_{m0} for a distortion of ~6 nm; e_m is influenced by detachment of motors at $\Delta z > 6$ nm; (4) at the end of the 100 μs stretch the relation between e_m/e_{m0} and Δz lies slightly but not significantly above that at 2 ms. These results support the idea that stretch-induced sliding of the actin filament distorts the actin-attached motor domain of the myosin dimers away from the centre of the sarcomere, providing the steric conditions for rapid attachment of the second motor domain. The rate of new motor attachment must be as high as 7.5×10^4 s^{-1} and explains the rapid and efficient increase of the resistance of active muscle to stretch.

(Received 8 July 2009; accepted after revision 27 November 2009; first published online 30 November 2009)
Corresponding author V. Lombardi: Laboratorio di Fisiologia, Dipartimento di Biologia Evoluzionistica, Università di Firenze, Via G. Sansone 1, 50019 Sesto Fiorentino, Italy. Email: vincenzo.lombardi@unifi.it

Abbreviations *h*s, half-sarcomere; T_0, isometric tetanic force; e, half-sarcomere stiffness; e_0, half-sarcomere stiffness at T_0; C_f, myofilament compliance; e_m, motor array stiffness; e_{m0}, motor array stiffness at T_0; Δz, distortion of the myosin motor; M3, third order of the myosin-based meridional reflections; I_{M3}, intensity of M3; R_{M3}, ratio of the intensities of the higher and lower angle peaks of M3.

Introduction

In skeletal muscle the motor protein myosin II has two identical S1 fragments or heads, of which only one at a time interacts with actin during isometric contraction or shortening. The functional significance of the dimeric structure of this molecular motor has not yet been well defined, even though the role of the second motor domain of the muscle myosin has been clarified in some respects during the last decade, with respect to ATP-driven work production (Davis & Rodgers, 1996; Huxley & Tideswell, 1997; Conibear & Geeves, 1998; Tyska *et al.* 1999; Smith *et al.* 2008), and braking action during forcible stretch (Brunello *et al.* 2007; Bekyarova *et al.* 2008). In particular, coordination of the action of the two heads has been hypothesized in models (Davis & Rodgers, 1996; Huxley & Tideswell, 1997) aimed at explaining the mechanical responses to rapid temperature jumps (Davis & Rodgers, 1995) or to double length steps (Lombardi *et al.* 1992). The braking action of muscle consists of a high resistance to lengthening when the load on the active muscle is increased above the steady force developed during an isometric contraction (T_0) (Katz, 1939). The response occurs at reduced metabolic cost (Infante *et al.* 1964; Curtin & Davies, 1973; Linari *et al.* 2003) and is characteristic of eccentric contractions, a condition that is quite common in normal life, such as when the extensor muscles of the legs have to resist the momentum of the body landing at the end of a jump. Step or ramp stretches superposed on isometric contraction produce increases in the stiffness of muscle fibres (Bressler *et al.* 1988; Sugi & Tsuchiya, 1988; Lombardi & Piazzesi, 1990; Mantovani *et al.* 1999; Linari *et al.* 2000*a*). When the stretch is imposed within the range of sarcomere lengths corresponding to

DOI: 10.1113/jphysiol.2009.178137

the plateau of the force–length relation (2–2.25 μm for frog muscle fibres (Edman, 1966; Gordon *et al.* 1966)) and under the condition that the sarcomere homogeneity along the muscle fibre is preserved, recruitment of elastic structures in parallel to the contractile elements of the sarcomere (Edman *et al.* 1982; Morgan, 1990, 1994; Noble, 1992; Edman & Tsuchiya, 1996; Herzog & Leonard, 2002; Linari *et al.* 2003) can be excluded. Thus, the increase in stiffness can be attributed either to non-linearities in the stress–strain relation of the contractile elements (myosin filament, actin filament and myosin motors attached to actin) or to an increase in the number of myosin motors working in parallel in each half-sarcomere.

The compliances of the myosin and actin filaments have been estimated from X-ray diffraction measurements of the filament periodicities at different forces (Huxley *et al.* 1994, 2006*b*; Wakabayashi *et al.* 1994; Dobbie *et al.* 1998; Bordas *et al.* 1999; Piazzesi *et al.* 2002, 2007; Reconditi *et al.* 2004; Tsaturyan *et al.* 2005). Apart from the relatively large ($\sim$1%) spacing changes of these reflections accompanying activation and steady shortening at low load (attributed to a structural rearrangement of the filaments), there is a general consensus that the elastic extensibility of both the myosin and the actin filaments is 0.23–0.26% ${T_0}^{-1}$. From these values, applying a distributed filament compliance analysis (Ford *et al.* 1981) to muscle fibres from *Rana temporaria* at 2.2 μm sarcomere length (temperature $\sim$4°C, T_0 250–300 kPa), a cumulative equivalent myofilament compliance (C_f) of 3.4–3.8 nm ${T_0}^{-1}$ can be calculated. This value corresponds to 12–14 nm MPa^{-1}, taking a T_0 value of $\sim$280 kPa. Similar values for C_f (12–13 nm MPa^{-1}) are obtained from purely mechanical experiments (Brunello *et al.* 2006; Piazzesi *et al.* 2007; Linari *et al.* 2009). In all those X-ray and mechanical experiments the contribution of the myofilaments to the half-sarcomere compliance was that of a linear elasticity. Larger changes in the periodicities of the filaments have only been reported for conditions that involve a change in filament structure, either for actin (Bordas *et al.* 1999; Linari *et al.* 2005; Tsaturyan *et al.* 2005) or myosin (Huxley *et al.* 2006*b*; Piazzesi *et al.* 2007).

Further evidence for a linear elasticity of the myofilaments is provided by stiffness measurements in skinned fibres from mammalian muscle in rigor (Higuchi *et al.* 1995; Linari *et al.* 2007). Under this condition all myosin motors are attached to the actin filament (Cooke & Franks, 1980; Thomas & Cooke, 1980; Lovell *et al.* 1981), so that stress–strain relations can be determined at different steady forces without change in the number of attached motors. Apart from at very low forces, where the estimate may be influenced by filaments becoming slack (Higuchi *et al.* 1995), these stress–strain relations have the same slope, independent of the steady force level (Linari *et al.* 2007).

It was recently suggested that force dependence of myofilament stiffness might explain the effect of sarcomere length on the relation between half-sarcomere stiffness and force (Edman, 2009). However, calculations by one of us (Reconditi, 2010) show that these data can be fitted equally well by a constant myofilament compliance.

An alternative explanation for the increase in stiffness on stretch is that the myosin motors themselves exhibit non-linear elasticity. Several lines of evidence support the view that the stress–strain relation of an attached myosin motor is not sensitive to the level of force or the distortion of the motor itself. In intact fibres from the frog, the force of the myosin motor can be modulated by temperature by a factor of almost two without any change of the motor stiffness (Piazzesi *et al.* 2003; Decostre *et al.* 2005). Moreover, in contrast with a previous view (Fajer *et al.* 1988; Pate & Cooke, 1988), it has recently been demonstrated that the stiffness of each motor remains unchanged even when, as in rigor, both heads of the same myosin molecule are attached at the same time (see Fig. 8 in Linari *et al.* 2007).

The first evidence that the increase of stiffness on stretch is due to attachment of new motors came from the comparison of the stiffness changes following a step stretch of 3–4 nm per half-sarcomere (hs) superimposed on isometric contraction or the steady force response to ramp lengthening (Colomo *et al.* 1987). More recently evidence for stretch-dependent attachment of myosin motors was derived from studies of the X-ray interference between the two arrays of myosin motors in each thick filament (Huxley & Brown, 1967; Linari *et al.* 2000*b*), a method that allows the axial movement of the myosin motors to be measured directly (Piazzesi *et al.* 2002; Reconditi *et al.* 2004; Huxley *et al.* 2006*a*). In this respect it must be noted that, in all the work published on this subject since Piazzesi *et al.* (2002) (Reconditi *et al.* 2004; Huxley *et al.* 2006*a*,*b*; Brunello *et al.* 2007; Piazzesi *et al.* 2007), the estimate of the axial movement of attached heads from the X-ray interference changes has taken into account the contribution of detached heads, as later claimed by Knupp *et al.* (2009).

It has been found that, following stretches of 2–6 nm hs^{-1} imposed on isometrically contracting fibres from frog muscle, the increase in the interference distance between the two motor arrays is less than expected from the amount of distortion imposed on the motors by the stretch (Brunello *et al.* 2007). This phenomenon occurs on the 100 μs time scale of the stretch. Together with the finding that stiffness increases further during the drop in force following the end of the stretch, the X-ray data argued against a contribution to the stiffness increase from non-linear elasticity of myofilaments. The results could be explained by assuming that the unattached motor domains of the myosin dimers, with a motor domain already attached to an actin monomer, bind to the next monomer, 5.5 nm further from the Z-line. The precise

mechanism of the attachment of the second motor and its kinetics remained to be established.

Here the mechanism of motor recruitment by stretch is investigated using fast half-sarcomere mechanics in single fibres. We measure the changes in the stiffness of the motor array both at the end of and following stretches (complete in 100 μs) of 2–8 nm hs^{-1}, superimposed on the isometric tetanic force (T_0). Half-sarcomere stiffness is also measured after induction of rigor, in the same range of steady forces as those explored when stretching active fibres. In this way it is possible to check whether any non-linear elasticity in the myosin motors and myofilaments contributes to the stiffness increase. The results show that: (i) the half-sarcomere stiffness in rigor is constant independent of the force level; (ii) at 2 ms following a stretch imposed on an active fibre, the increase in stiffness of the motor array with respect to the isometric value (e_m/e_{m0}) and thus the extent of recruitment of new motors has a sigmoidal dependence on the distortion of the first head, Δz (measured as the axial shift between the catalytic domain attached to actin and the head–rod junction, with $\Delta z = 0$ in isometric contraction and positive for a Z-ward shift) and attains a maximum value of ~2; (iii) the relationship between e_m/e_{m0} and Δz at the end of the stretch (100 μs) lies slightly but not significantly above that at 2 ms following the stretch.

Methods

Ethical approval, fibre preparation and mechanical apparatus

Single fibres were dissected from the lateral head of the tibialis anterior muscle of *Rana esculenta* after killing by decapitation followed by destruction of the brain and the spinal cord according to the European Community Country Directive 86/609/EEC and in conformation with the indications of the Institutional Animal Care and Use Committee of the University of Florence, and the UK Animals (Scientific Procedures) Act 1986 (Drummond, 2009). Fibres were transferred to a thermo-regulated trough and mounted between a capacitance force transducer with resonant frequency of ~50 kHz (Huxley & Lombardi, 1980) and a loudspeaker motor (Lombardi & Piazzesi, 1990), by means of aluminium clips fixed to the tendons (Ford *et al.* 1977). Sarcomere length was set at 2.15 μm. A striation follower (Huxley *et al.* 1981) continuously recorded the sarcomere length changes in a 1.0–1.5 mm segment at the fibre end close to the force transducer, with a sensitivity of 100 mV nm^{-1} hs^{-1}.

The physiological Ringer's solution bathing the fibre (115 mM NaCl, 2.5 mM KCl, 1.8 mM $CaCl_2$, 3 mM phosphate buffer, pH 7.1) was kept at 4°C by means of a servo-controlled thermoelectric module.

The rigor state was induced by adding metabolic poisons (1 mM iodoacetic acid, 5.6 mM 2,4-dinitrofluorobenzene and 1 mM sodium azide) to Ringer's solution cooled to 1°C and containing 20 mM butanedione monoxime (BDM). The development of rigor was monitored by means of stiffness measurements. After complete rigor development, fibres were returned to Ringer's solution with BDM, then to Ringer's solution. With this procedure (Piazzesi *et al.* 2007) sarcomere order and strong tendon attachments are preserved.

Experimental protocol

Fibres were electrically stimulated to develop fused tetanic responses at 4 min intervals, using stimuli of alternating polarity with frequency of 18–25 Hz and 0.5 s duration. After 0.35 s of isometric contraction, when force had attained the tetanus plateau (T_0), a step increase in length (range 2–8 nm hs^{-1}, rise time 90 μs) was imposed on the fibre. The upper limit of the stretch size was set according to the observation that often, following stretches larger than 8 nm hs^{-1}, the stiffness determined at the isometric tetanus plateau was irreversibly reduced, indicating damage in some half-sarcomere components. The stiffness of the fibre following the stretch was measured by imposing test length steps (±1 nm hs^{-1}) just before and 2 ms after the conditioning stretch. In the range 1–6 nm hs^{-1}, the stiffness was continuously measured before and after the stretch by imposing small (*ca* 1 nm hs^{-1} peak to peak) length oscillations at 4 kHz.

Stiffness in rigor was measured at different steady forces in the range of 0.5–1.5 T_0 (where T_0 was determined for each fibre before rigor induction), obtained by imposing slow ramp stretches to rigor fibres starting from the low level of force (<0.1 T_0) developed at the end of the rigorization procedure. The amplitude of the stretch (3–8 nm hs^{-1}) was adjusted to achieve the steady force at which the stiffness was measured by imposing a train of different-sized length steps (ranging from +3 to −3 nm hs^{-1}), at intervals of 200 ms (Fig. 1*A* and *B*). To maintain the force before the test step constant, each test step was followed, after 50 ms, by a step of the same size in the opposite direction. The outputs from the force transducer, the striation follower and the loudspeaker motor were recorded (acquisition rate 200 kHz) with a multifunction I/O board (PCI-6110E, National Instruments) and a program written in LabVIEW (National Instrument). A total of 13 muscle fibres with cross-sectional area of 8700 ± 2000 μm^2 (mean ± S.D.) and isometric force (T_0) of 152 ± 8 kPa were used.

Data analysis

Rigor fibres. Half-sarcomere stiffness at each steady force level was estimated by the slope of the relation between the

force attained at the end of the step and the half-sarcomere length change (Fig. 1*C*).

Active fibres. Data obtained either at the peak of force attained at the end of the conditioning stretch (phase 1) or at 2 ms following the stretch (phase 2) were grouped into six classes on the basis of the size (ΔL) of the conditioning stretch (1 nm hs^{-1} classes for $1 < \Delta L < 5$ nm hs^{-1} and 2 nm hs^{-1} classes for $\Delta L > 5$ nm hs^{-1}) and averaged. For phase 1, two further classes (-1–0 and 0–1 nm hs^{-1}) were defined by collecting the data obtained from the small test releases and stretches used to measure the isometric half-sarcomere stiffness in each experiment. Errors are S.E.M., unless otherwise specified.

The distortion of the isometric motors induced by the stretch is calculated as:

$$\Delta z = \Delta L - C_{\mathrm{f}} \times \Delta T$$

where ΔL and ΔT are the half-sarcomere length change and the force change, respectively, and C_{f} is the filament compliance, calculated, for the fibres used in this series of experiments, from the slope of the relationship between half-sarcomere strain and force during isometric force development (see Fig. 3 and for reference, Brunello *et al.* 2006).

Half-sarcomere stiffness and motor array stiffness in phase 1 were determined as the slope of the segments connecting two consecutive T_1 points in the T_1–ΔL and T_1–Δz relations, respectively. The increase in motor array stiffness with respect to the isometric value was calculated as

$$\frac{e_m}{e_{m0}} = \frac{C_{\mathrm{hs0}} - C_{\mathrm{f}}}{C_{\mathrm{hs}} - C_{\mathrm{f}}}$$

where $C_{\mathrm{hs0}}(=1/e_0)$ is the half-sarcomere compliance during isometric contraction and $C_{\mathrm{hs}}(=1/e)$ the half-sarcomere compliance after the conditioning step.

The 4 kHz oscillation responses were analysed by means of a program written in LabVIEW that calculates the Fourier transform of length and force signals, extracting amplitude and phase of the oscillations. The complex stiffness (E) is calculated as the ratio of the amplitudes of force and length oscillations. The real part of the complex stiffness is the elastic stiffness $e = E \times \cos(\Delta\varphi)$, while the imaginary part is the viscous stiffness $\eta = E \times \sin(\Delta\varphi)$, where $\Delta\varphi$ is the phase shift between the force and length oscillations. With 4 kHz oscillations, at T_0 $\Delta\varphi$ was $\sim$0.1 rad and it changed by less than 0.1 rad within the limits of the experimental conditions explored in this work; thus, e practically coincides with E and can be used as a reliable estimate of the stiffness of the undamped elasticity in the half-sarcomere.

Results

Stiffness in rigor

When a length step of a few nanometres per half-sarcomere, complete in 100 μs, is imposed on the steady force level of a fibre in rigor, the force changes during the step to a value T_1 and then exhibits only a very small recovery on the timescale of a few milliseconds (Fig. 1*B*). The force T_1 is due to the undamped elastic properties of the half-sarcomere components: the myosin filament, the actin filament and the array of actin-attached myosin motors. In Fig. 1*C*, the force attained at the end of the length step is plotted *versus* the sarcomere length change for two different steady forces (114 kPa, circles, and 209 kPa, triangles). The isometric tetanic force T_0 in the active fibre was 142 kPa. It can be seen that all the T_1 points belonging to the same steady force lie on a straight line independent of the step size and the level of force, even for forces up to 355 kPa or 2.5 T_0. The slopes of the linear fits that measure the half-sarcomere stiffness are practically the same, 0.424 ± 0.013 T_0 nm^{-1} for the circles and 0.415 ± 0.004 T_0 nm^{-1} for the triangles. Figure 1*D* shows the relation between the half-sarcomere stiffness, expressed as the Young's modulus ($(\Delta T/\mathrm{CSA}) \times (\mathrm{hs\ length}/\Delta L)$) and the steady force obtained from the four fibres used for the rigor protocol. The linear regression equation fitted to the stiffness data has a slope not significantly different from zero (-4 ± 12) and its ordinate intercept is 69 ± 2 MPa. These results indicate that in rigor the myosin motors and the myosin and actin filaments exhibit linear elasticities in a range of steady forces up to 275 kPa.

Stiffness changes during stretch of the active fibre

When a stretch of a few nanometres per half-sarcomere, complete in 100 μs, is imposed on the plateau of an isometric tetanus (force T_0), the force increases to a value T_1 during the stretch and then partially recovers (Fig. 2*A*). As in the case of the response to a length step in rigor, the force increase during the stretch is mainly due to the undamped elastic properties of the myofilaments and the actin-attached myosin motors. However, in contrast to the rigor results (Fig. 1*C*), the relation between T_1 and the size of the stretch (Fig. 2*B*, filled circles) deviates from linearity, so that T_1 points for steps larger than 1 nm hs^{-1} lie above the linear relation (continuous line) extrapolated from the ± 1 nm hs^{-1} steps and the isometric point (see also Ford *et al.* 1977; Lombardi & Piazzesi, 1990). The slope of the continuous line estimates the half-sarcomere stiffness at T_0 (e_0) and is 0.263 ± 0.001 T_0 nm^{-1} (9 fibres, Fig. 2*C*). With $T_0 = 139 \pm 7$ kPa, the Young's modulus in these fibres is 39 ± 2 MPa, not significantly different from

previous estimates in the same preparation (Piazzesi *et al.* 2003; Decostre *et al.* 2005).

The progressively larger deviation of the T_1 points from the continuous line indicates a progressive increase in the half-sarcomere stiffness, e, as expected from the recruitment of new motors during the step itself (Brunello *et al.* 2007). The stretch-dependent increase in half-sarcomere stiffness relative to the isometric value (e/e_0) is estimated here by the change in the slope of the straight line joining two consecutive T_1–ΔL points (open circles in Fig. 2*B*, with the abscissa value corresponding to the centre of the ΔL segment). The same analysis, repeated for the nine fibres, is shown in Fig. 2*C*. In this case, for each e/e_0, the abscissa value is the mean of the centred values

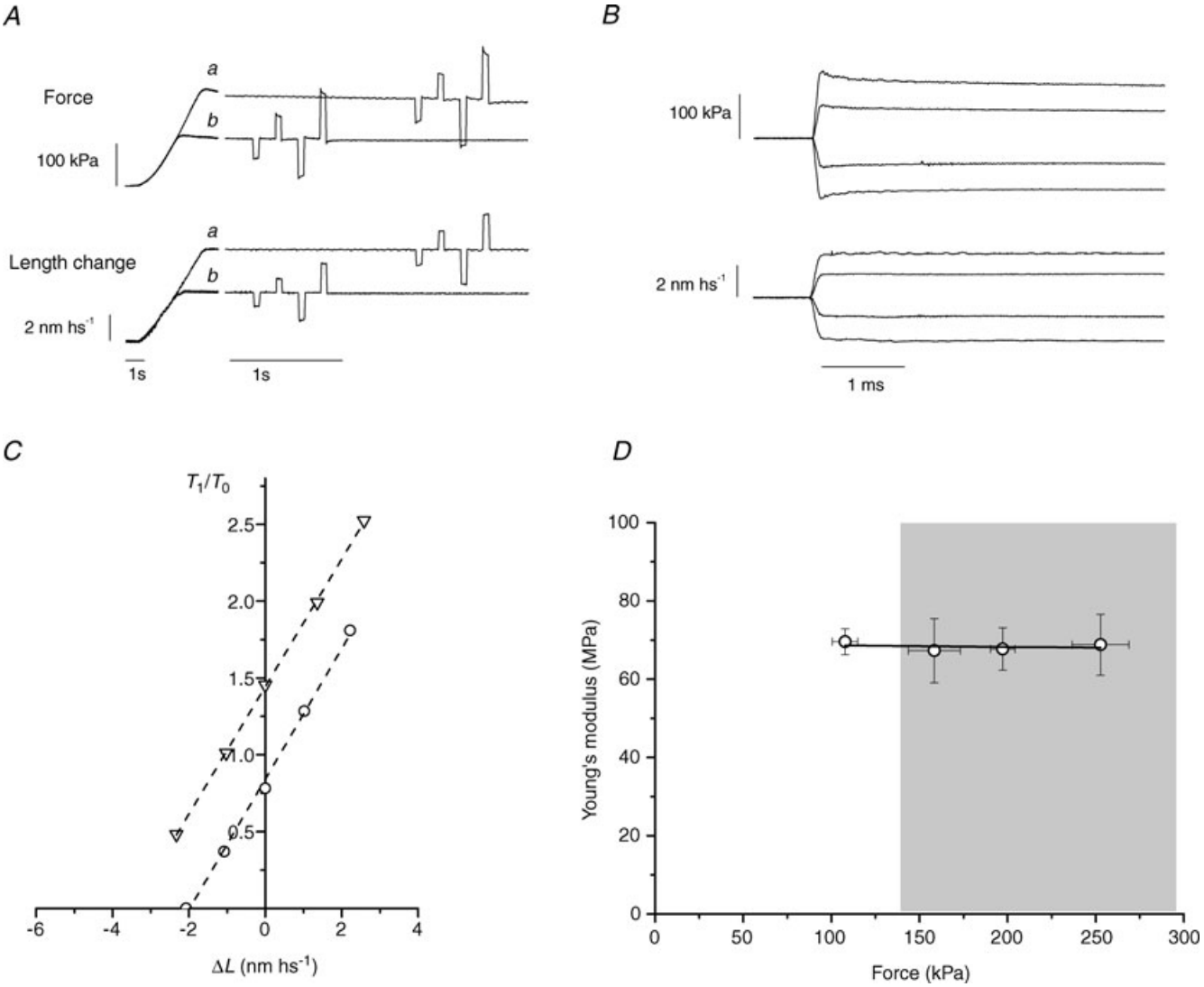

Figure 1. Half-sarcomere stiffness in rigor

A, force responses (upper traces) to a sequence of four step length changes (lower traces) imposed at 200 ms intervals on steady forces (*a*, 209 kPa; *b*, 114 kPa) attained with two different amounts of slow lengthening of the fibre in rigor. The time base is changed in correspondence of the interruption of the traces according to the calibrations. Step amplitudes were about ±1 and ±2 nm hs^{-1}. A step of opposite polarity was imposed after each test step to return the force to its value before the test step. *B*, superimposed force responses (upper traces) and length changes (lower traces) from record *Aa* at a faster time base. *C*, T_1 relations (relative to the isometric tetanic force T_0, 142 kPa) from the records in *A*. Dashed lines are the linear fits to data: the slopes are 0.424 ± 0.013 T_0 nm^{-1} for the circles and 0.415 ± 0.004 T_0 nm^{-1} for the triangles. *D*, Young's modulus (MPa) of the half-sarcomere in rigor at different steady force levels. Data from 4 fibres are grouped into 4 classes of steady force; errors are S.D. Continuous line is the linear fit to data, with slope −4 ± 12 and intercept 69 ± 2 MPa. Grey rectangle indicates the range of forces where stiffness was measured during active contraction (from 139 kPa, the average T_0 in the 9 fibres used for the stretch experiments, to the maximum force at T_2, 297 kPa, attained with the stretch of ∼8 nm hs^{-1}).

of the respective ΔL segments. In the range of ΔL from 0.5 to 8 nm hs^{-1}, e/e_0 increases from 1.03 ± 0.01 to 1.24 ± 0.07.

The increase in the stiffness of the array of motors attached to actin in each half-sarcomere can be estimated from the half-sarcomere stiffness changes only after taking into account the contribution of the myofilament compliance (C_f). In mechanical experiments, C_f can be estimated from the change in half-sarcomere strain under conditions where the force changes at constant strain of the myosin motors, such as during the rise of the isometric force in a tetanus (Brunello *et al.* 2006) or when force is modulated by N-benzyl-p-toluene sulfonamide (BTS) (Linari *et al.* 2009). C_f for the fibres used in these experiments was estimated by determining the relation between half-sarcomere strain and force during the rise of the isometric tetanus. Length oscillations of 4 kHz (<2 nm hs^{-1} peak to peak) were applied during the rise of force (Fig. 3*A*). The half-sarcomere stiffness was calculated from the complex stiffness obtained by analysing 10 consecutive cycles at different levels of force. The half-sarcomere strain ($Y_0 = (T/T_0)/e$, filled circles in Fig. 3*B*) increases linearly during force development and the slope of the linear regression on the data (continuous line) is 1.77 ± 0.05 nm T_0^{-1}. Taking into account the value of T_0 in this experiment (150 kPa), the slope is 11.8 ± 0.3 nm MPa^{-1}, a value in agreement with the contribution of myofilament compliance (C_f) to half-sarcomere compliance estimated from previous mechanical and X-ray measurements (Huxley *et al.* 1994; Wakabayashi *et al.* 1994; Dobbie *et al.* 1998; Reconditi *et al.* 2004; Brunello *et al.* 2006; Piazzesi *et al.* 2007; Linari *et al.* 2009). The ordinate intercept of the linear regression, 1.83 ± 0.04 nm, is the average strain of the attached myosin motor (s), and remains constant during the development of isometric force in this force range, as shown by the open circles (Fig. 3*B*) obtained by subtracting the filament strain from half-sarcomere strain. In three fibres, C_f was 1.91 ± 0.07 nm T_0^{-1} or 12.3 ± 0.4 nm MPa^{-1} and s was 1.76 ± 0.05 nm.

Comparison with the previous work quoted above shows that, while the maximum isometric strain of the filaments varies by a factor of almost 2 due to variation of T_0 in different species and batches of frogs (with fibres from *Rana temporaria* in the upper range of forces (250–300 kPa at 4°C) and fibres from *Rana esculenta* in the lower range (130–180 kPa at 4°C)), C_f is the same, as expected elasticity of the actin and myosin filaments is linear. Moreover, the motor strain s is in agreement with the values estimated by different methods in previous work at the same temperature (Decostre *et al.* 2005; Piazzesi *et al.* 2007). This indicates that T_0 at a given temperature varies between species and batches of frogs mainly because of the variation in the number of motors working in parallel in the half-thick filament.

Knowing C_f, the amount of motor distortion (Δz) at any time following a step in half-sarcomere length can be calculated by subtracting the contribution of filament strain ($C_f \times \Delta T$, where ΔT is the increase of force above T_0) from ΔL (Fig. 2*A*). The calculation is equally valid for the high forces attained with the stretches, because the elasticity of the half-sarcomere is linear for forces up to 2.5 T_0. In Fig. 4*A* the T_1 data from Fig. 2*B* are plotted against Δz. The stiffness of the motor array at T_0 (e_{m0}) is estimated as the slope of the straight line through the T_1–Δz points for the smallest steps (ΔL *ca* ±1 nm hs^{-1})

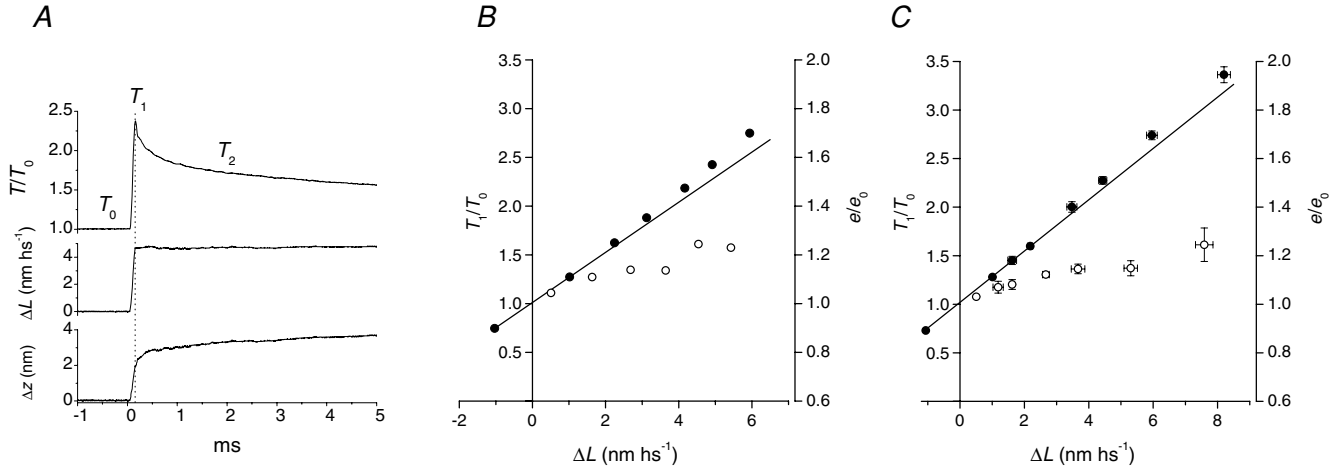

Figure 2. Half-sarcomere stiffness during a stretch
A, force and average motor distortion in response to a step stretch imposed during isometric contraction. Upper trace, force (T) relative to isometric force (T_0); middle trace, length change (ΔL, nm hs^{-1}); lower trace, axial distortion of myosin motors (Δz, nm). *B*, relations of T_1/T_0 (filled circles) and e/e_0 (open circles) *versus* ΔL for one fibre. The continuous line is the linear fit to T_1/T_0 data for $\Delta L = \pm 1$ nm hs^{-1}, the slope (e_0) is 0.26 T_0 nm^{-1}. *C*, average T_1/T_0 and e/e_0 relations for 9 fibres (mean ± S.E.M.); the continuous line is calculated as in *B*, the slope is 0.263 ± 0.001 T_0 nm^{-1}. T_0 in these experiments was 139 ± 7 kPa (mean ± S.E.M.).

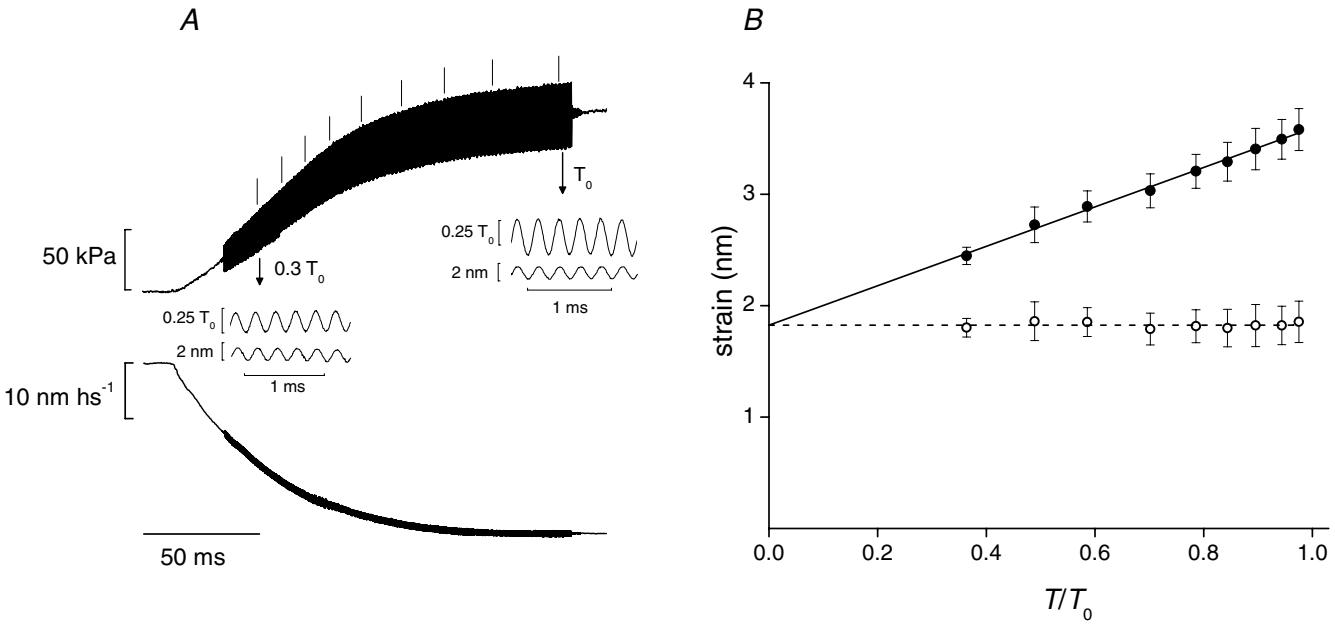

Figure 3. Measurement of myofilament compliance
A, force (upper trace) and half-sarcomere length change (lower trace) during the development of the isometric tetanus with superposed 4 kHz length oscillations (~2 nm hs^{-1} peak to peak) applied starting from 0.2 T_0. Stiffness was calculated in correspondence of the vertical bars above the force trace. The insets show force response (upper trace) and length oscillations (lower trace) on a faster time scale at 0.3 T_0 and T_0, as indicated by the arrows. *B*, half-sarcomere strain (filled circles) and motor strain (open circles) plotted against force relative to T_0. The continuous line is the linear regression on strain–force data (mean ± S.D., 1 fibre, $T_0 = 150$ kPa) with a slope 1.77 ± 0.05 nm T_0^{-1} and ordinate intercept 1.83 ± 0.04 nm. Dashed line is $y = 1.83$ nm.

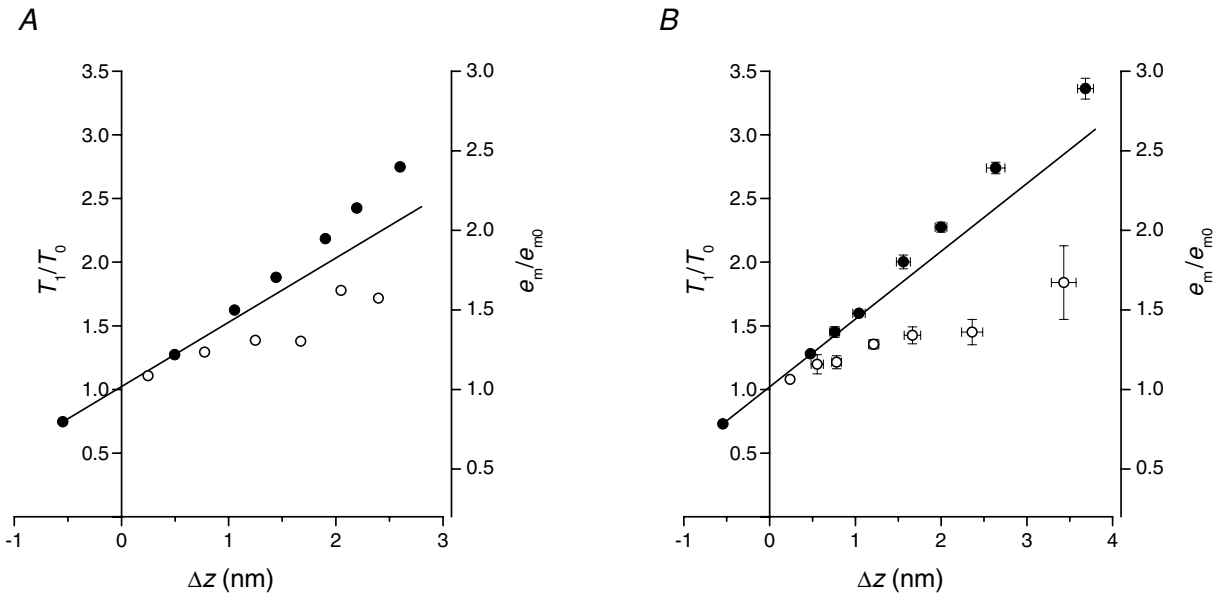

Figure 4. Stiffness of the motor array during a stretch
A, relations of T_1/T_0 (filled circles) and e_m/e_{m0} (open circles) against Δz. The continuous line is the linear fit to T_1/T_0 data for $\Delta z = \pm 0.5$ nm; the slope (e_{m0}) is 0.51 T_0 nm^{-1}. Data from the same fibre as in Fig. 2*B*. *B*, average T_1/T_0 (filled circles) and e_m/e_{m0} (open circles) relations for the 9 fibres (mean ± S.E.M.) as in Fig. 2*C*; the slope of the line, calculated as in *A*, is 0.527 ± 0.005 T_0 nm^{-1}.

and the isometric point. As in the case of Fig. 2*B*, the increase in the stiffness of the motor array with Δz is given by the change in slope of the T_1–Δz relation and is calculated as the slope of the segment joining two consecutive T_1 points divided by e_{m0} (e_m/e_{m0}, open circles in Fig. 4*A*, with the abscissa value corresponding to the centre of the Δz segment). Mean values for the nine fibres are shown in Fig. 4*B*. In the range of Δz from 0.2 to 3.5 nm e_m/e_{m0} increases from 1.07 ± 0.01 to 1.67 ± 0.23, without a clear sign of saturation.

Stiffness changes during the quick force recovery following a stretch

Force recovery in the first 2 ms following a stretch is attributed to the reversal of the working stroke in the myosin motors attached to actin in isometric contraction (Ford *et al.* 1977; Piazzesi *et al.* 1997). This process is accompanied by a further increase of Δz and the recoil of filament compliance (Fig. 1*A*).

In Fig. 5 the stiffness changes following the stretch are estimated by superposing small (~1 nm hs^{-1} peak to peak) 4 kHz oscillations on the length step and determining the amplitude ratio of the change in force to the change in length (see Methods). To eliminate the distortion of the oscillations by the rapid force transient accompanying the step, the stiffness measurements are made on the traces (*b* and *d*) obtained after subtracting the response to the step alone from the response to the step plus oscillations (*a* and *c*). Moreover, each stiffness value (*e*) is calculated from the average of three cycles, so that the first reliable stiffness measurement after the step start is at 625 μs (thicker part of trace in *b* and *d*, and filled symbols in *e*). At this time, for each stretch size, the increase in stiffness has already attained its maximum value, which is larger for larger stretches. Stiffness then reduces with a time course slower than the force recovery, in agreement with the rate of motor detachment–reattachment estimated with the double-step protocol (Piazzesi *et al.* 1997). The resolution of the half-sarcomere length signal required for reliable stiffness measurements is quite high, and we obtained enough statistics for conditioning stretches of up to 5 nm hs^{-1}. For the 6 nm hs^{-1} stretch (diamonds), the e/e_0 points are only from one experiment and are not used for the subsequent analysis.

The dependence of the stiffness increase on the stretch size was further investigated in the range 2–8 nm hs^{-1} by imposing small ($\pm$1 nm hs^{-1}) length steps at 2 ms during the quick force recovery following the stretch (Fig. 6*A*). At 2 ms, the stiffness increase induced by the stretch is

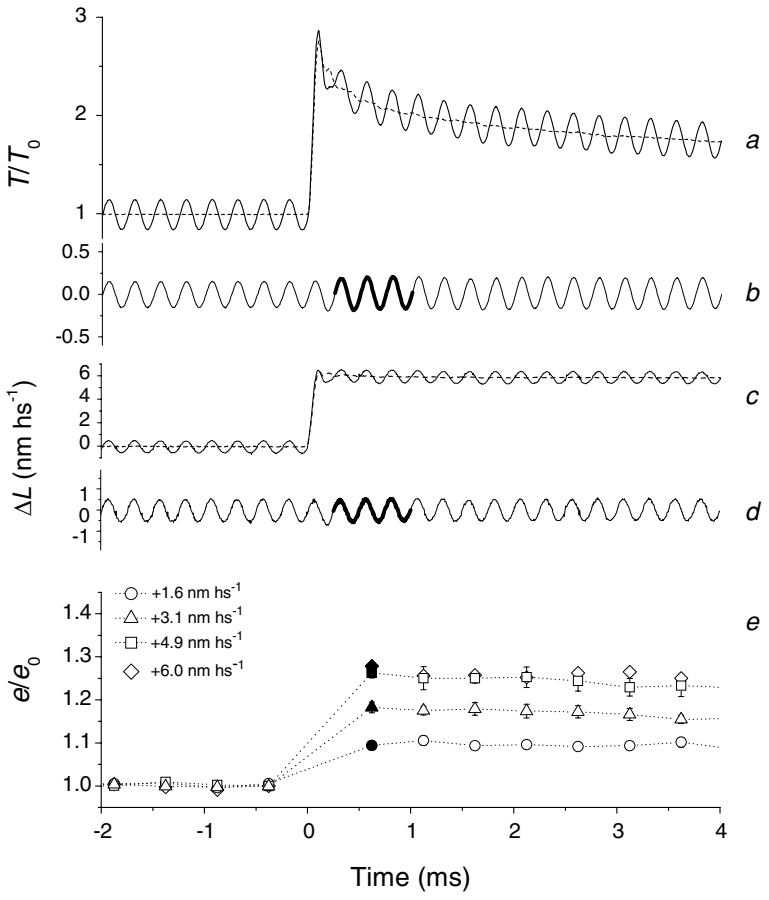

Figure 5. Stiffness measurements with 4 kHz length oscillations
Force response (*a*) to a 6 nm hs^{-1} stretch (*c*) with (continuous lines) and without (dashed lines) superimposed 1 nm hs^{-1} peak-to-peak 4 kHz length oscillations. Traces *b* and *d* were obtained after subtracting the responses without oscillations from those with oscillations. Half-sarcomere stiffness for four step sizes (1.6 nm hs^{-1}, circles; 3.1 nm hs^{-1}, triangles; 4.9 nm hs^{-1}, squares; 6 nm hs^{-1}, diamonds) is shown in *e*. The first stiffness points after the step (filled symbols at 625 μs) are obtained from the three cycles as indicated by the thicker parts of traces in *b* and *d*. Data are mean ± S.E.M. from four fibres, except diamonds, which are from the fibre in *a*–*d*.

slightly reduced with respect to the maximum occurring at 0.62–1 ms (Fig. 5), but the 2 ms point was preferred to an earlier time because: (i) the fast phase of force recovery from the conditioning stretch is almost over and does not complicate the transient elicited by the test step and (ii) it is closer to the time window used for X-ray interference studies (Brunello *et al.* 2007).

The stiffness was estimated as the slope of the linear regression fit to both T_1 points for the test steps (Fig. 6*B*, open symbols) and the force attained just before the test step (T_i, filled symbols). Open circles in Fig. 6*C* show the relation between the half-sarcomere stiffness, relative to the value at T_0 (e/e_0), and ΔL for nine fibres. e/e_0 increases with the stretch size and tends to a plateau value just above 1.3 for the largest stretches. The stiffness of the motor array (e_m), calculated by subtracting the contribution of filament compliance from the measured stiffness (see Methods), increases with the stretch size

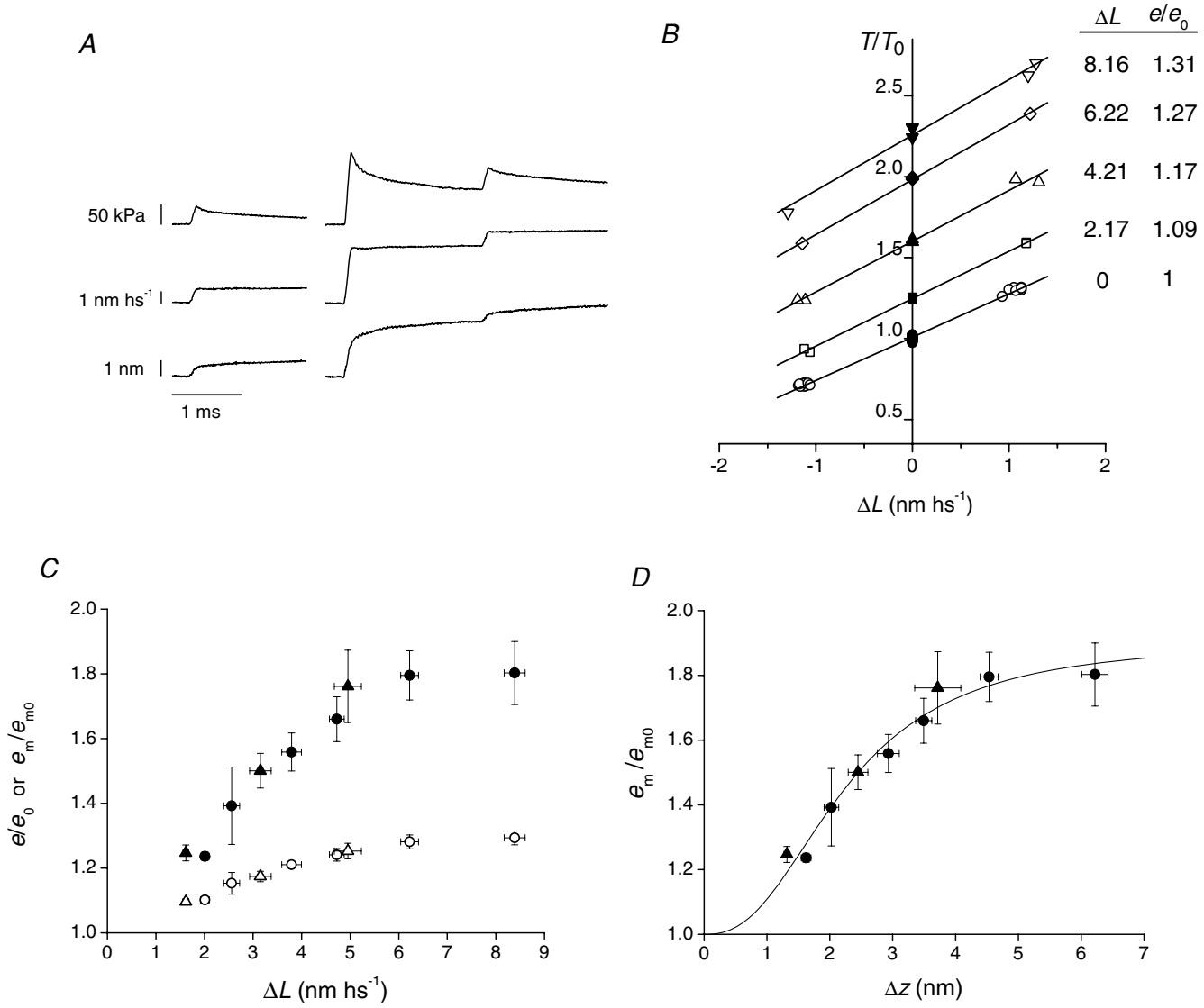

Figure 6. Stiffness measurements at 2 ms after the stretch
A, force response (upper trace) to length steps (middle trace) and average axial distortion of motors (Δz, lower trace). Test steps of amplitude ± 1 nm hs^{-1} were imposed at T_0 (left column) and at 2 ms after the conditioning stretch (right column). *B*, T_1 points for the test steps (open symbols) and T_i points (filled symbols, the force just before the test step) for T_0 (circles) and four different conditioning stretches of size ΔL, identified by the symbols as indicated in the table in the inset. e/e_0, reported in the table, are the slopes of the linear regressions (continuous lines) fitted to the T_1–T_i points, relative to that at T_0. Data from one fibre. *C*, e/e_0 (open circles) and e_m/e_{m0} (filled circles) obtained with the test steps at 2 ms after the stretch *versus* ΔL (mean ± S.E.M., 9 fibres). Open and filled triangles are the respective values obtained at 2 ms after the stretch with 4 kHz length oscillations (from Fig. 5). *D*, e_m/e_{m0} *versus* Δz at 2 ms after the stretch (same data as filled symbols in *C*). The continuous line is the data fit of the equation: $e_m/e_{m0} = A\,(\Delta z^n)/(k^n + \Delta z^n) + 1$.

reaching a maximum of ∼1.8 e_{m0} for ΔL of ∼8 nm hs^{-1} (Fig. 6*C*, filled circles). Filled triangles in Fig. 6*C* are the e_m/e_{m0} values estimated at 2 ms from the 4 kHz oscillation experiments (Fig. 5) and lie on the same relation as the filled circles, showing the consistency of the two methods.

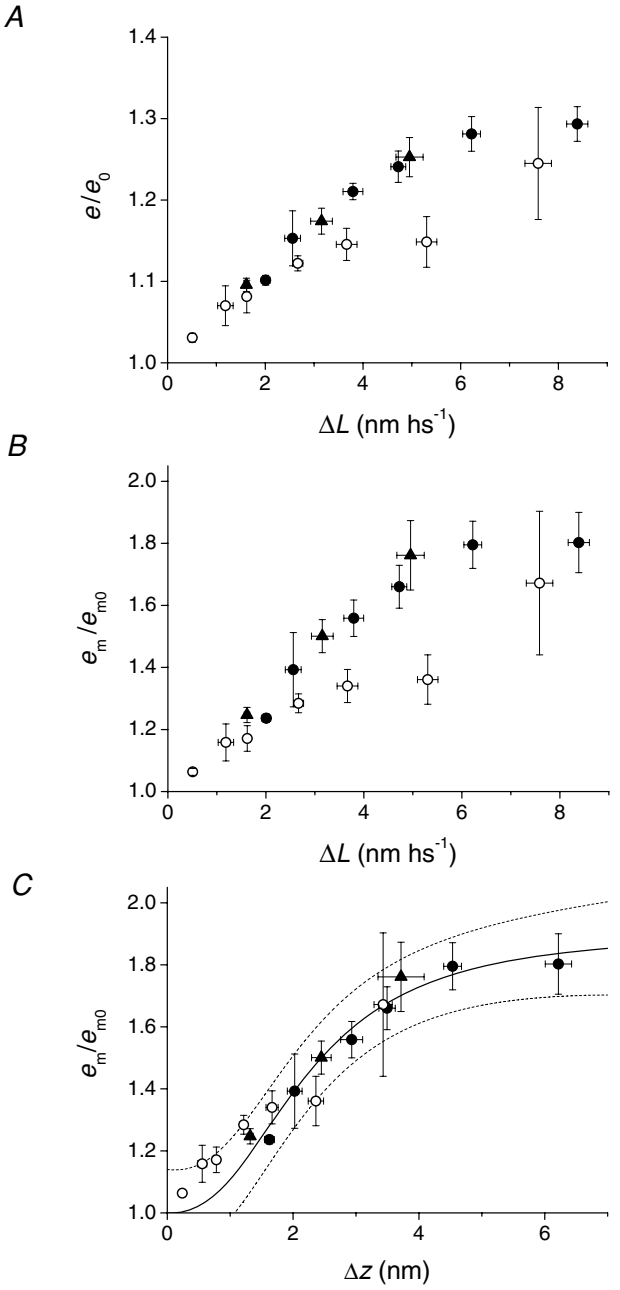

Figure 7. Comparison between stiffness of the motor array in phase 1 (open circles) and phase 2 (filled symbols)
A, relation of e/e_0 *versus* ΔL at the end of the stretch (open circles from Fig. 2*C*) and at 2 ms after the stretch (open symbols from Fig. 6*C*). *B*, relation of e_m/e_{m0} *versus* ΔL at the end of the stretch (from open circles in Figs 2*C* and 4*B*) and at 2 ms after the stretch (filled symbols from Fig. 6*C*). *C*, relation of e_m/e_{m0} *versus* Δz at the end of the stretch (open circles from Fig. 4*B*) and at 2 ms after the stretch (filled symbols and continuous line from Fig. 6*D*). Dashed lines are the prediction bands with a confidence level of 95%.

The relation between e_m and Δz at 2 ms following the stretch is shown in Fig. 6*D*. Data for small Δz values clearly point toward an abscissa intercept larger than zero, suggesting a sigmoidal relation. The continuous line is the fit to the points of the equation:

$$\frac{e_m}{e_{m0}} = \frac{A \cdot \Delta z^n}{\Delta z^n + k^n} + 1$$

where $(A + 1)$ is the asymptotic value of e_m/e_{m0}, k is the Δz value at which the increase of e_m/e_{m0} is half-maximum and n is the order of the reaction. From the fit, $A = 0.90 \pm 0.08$, $k = 2.25 \pm 0.21$ nm and $n = 2.46 \pm 0.45$.

Comparison between stiffness in phases 1 and 2

The comparison of the relations between e/e_0 (Fig. 7*A*) or e_m/e_{m0} (Fig. 7*B*) and ΔL in phase 2 (filled symbols) and in phase 1 (open symbols) shows that, in the ΔL range far from saturation ($\Delta L < 7$ nm hs^{-1}), the phase 2 relations show a larger slope than the phase 1 relations, even if for small stretches ($\Delta L < 3$ nm hs^{-1}) the ΔL dependence of either e/e_0 or e_m/e_{m0} is similar for the two phases.

For a given size of stretch, the amount of distortion (Δz) undergone by the motors is only about half of the stretch size in phase 1, due to the part of the length change taken by the myofilaments, but Δz increases in phase 2, as the force drops and the myofilament strain decreases (Fig. 2*A*). This explains why, when the e_m/e_{m0} data are plotted against Δz (Fig. 7*C*), the slope of the phase 1 relation (open circles from Fig. 4*B*) increases more than that of the phase 2 relation (filled symbols from Fig. 6*D*). Actually, for $\Delta z < 2$ nm, phase 1 points lie above phase 2 points, but the difference is not significant within the limits of the prediction bands with confidence level of 95% (dashed lines calculated from the sigmoidal fit (continuous line) to the phase 2 data).

We conclude that, for any Δz, independent of the time following the 100 μs stretch, the stiffness of the motor array depends only on the distortion of motors attached in isometric contraction. Provided that the stretch-induced increase in motor stiffness is due to recruitment of new motors (Brunello *et al.* 2007), this analysis shows that this process is sufficiently rapid to be at equilibrium by the time the stretch is complete.

Discussion

The increase in stiffness of the motor array is explained by actin attachment of new myosin motors

The stiffness of the array of myosin motors increases with Δz (the distortion of motors attached to actin in isometric contraction) during the stretch and continues to increase during the quick force recovery, when further

increase in Δz is generated by the recoil of filament elasticity accompanying the reversal of the working stroke. Actually, most of the Δz increase occurs within the first 500 μs following the end of the stretch, as the force drop and thus the recoil of filament elasticity are much faster early during phase 2 (Fig. 2*A*). This, together with the small counteracting effect of the slower process of motor detachment–attachment (the process of repriming from a stretch described in Piazzesi *et al.* (1997)), could explain why at 625 μs (Fig. 5) the stiffness increase is already at a maximum. It is worth considering that this influence of the repriming process on the motor recruitment is only possible because, although the rate of new motor attachment *per se* is several orders of magnitude larger than the rate of repriming, the increase in Δz following the stretch occurs at a progressively lower speed during the force recovery.

For the same value of Δz, the stiffness increase in phase 1 is slightly but not significantly higher than that in phase 2 (Fig. 7*C*). Previous work based on X-ray interference (Brunello *et al.* 2007) indicated that the increase in stiffness following a stretch is due to rapid attachment of the partner motor domain of myosin molecules with the first motor domain already attached in isometric contraction. This mechanism was suggested by the finding that the increase in distortion of the attached motor recorded by the change in X-ray interference is less than that expected from the imposed stretch, as is the case if attachment of new motors involves the actin monomers next to those already occupied by the attached motors, 5.5 nm further from the Z-line. The present work provides additional evidence that the stretch-dependent increase in stiffness of the active fibre cannot be attributed to non-linearity in the elasticity of either the myofilaments or the motor itself, but must be due to an increase in the number of motors. In the range of forces where the half-sarcomere stiffness at T_2 in the active fibre shows the maximum increase, the stiffness in the rigor state, when the number of attached motors is fixed, remains constant.

Consistency between mechanical and structural evidence for motor recruitment by stretch

Previous X-ray work (Brunello *et al.* 2007) concluded that for the same Δz the motor recruitment is larger in phase 1 than in phase 2, suggesting that the motor stress, which is larger in phase 1 than in phase 2, has a specific role in the process. This conclusion is not supported by the present mechanical data showing that the stiffness increase and thus the motor recruitment for the same Δz are not significantly different in the two phases.

Taking into account that no significant detachment–attachment of motors occurs during the first 2 ms following the stretch (Piazzesi *et al.* 1997), one would expect that the average axial shift of the centroid of the distribution of the actin-attached motors is the same, for the same Δz, in phases 1 and 2. In fact, the different stress of the attached motors (larger in phase 1 than in phase 2) is not *per se* a parameter that is able to affect substantially either the intensity of the myosin-based meridional reflection (M3) at 14.5 nm (I_{M3}) or its fine structure (the ratio of the intensities of the higher and lower angle peaks, R_{M3}). To test this idea, in Fig. 8 the R_{M3} (*A*) and I_{M3} (*B*) data from Brunello *et al.* (2007) are plotted *versus* their corresponding Δz values either in phase 1 (open circles) or in phase 2 (open triangles). It can be seen that both structural parameters tend to lie on a unique relation independently of the phase and thus of the stress of the motor. Note that in Brunello *et al.*

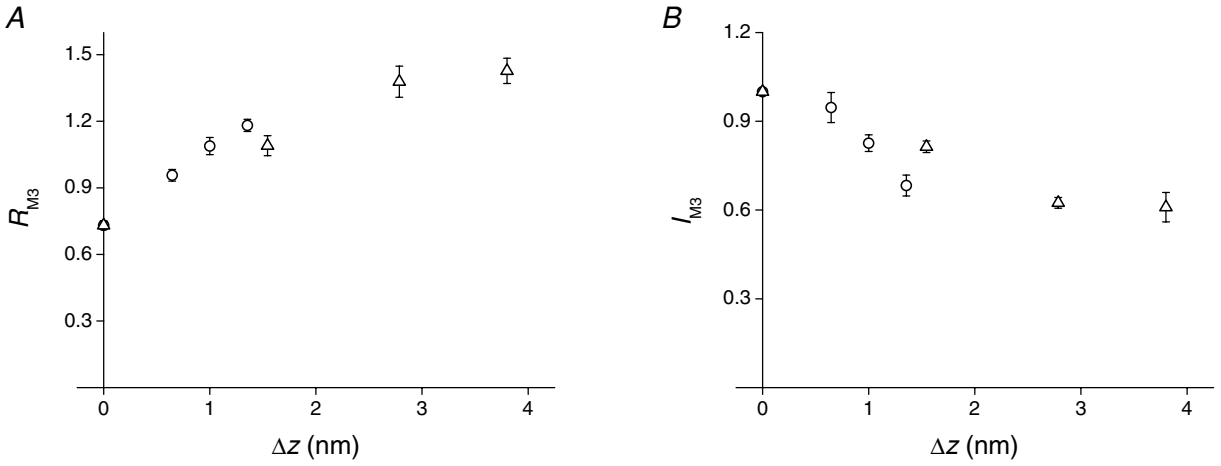

Figure 8. Dependence of R_{M3} and I_{M3} on motor distortion
A, R_{M3} values from Brunello *et al.* (2007) at the end of the stretch (circles) and at 2 ms after the stretch (triangles) plotted *versus* Δz values calculated using $C_f = 3.7$ nm T_0^{-1}. *B*, I_{M3} values from Brunello *et al.* (2007) plotted *versus* Δz. Symbols as in *A*.

(2007) the Δz values were calculated from ΔL values assuming a filament compliance (C_f) of 3.7 nm T_0^{-1}, corresponding to 13 nm MPa^{-1}, in agreement with the estimate in this work. This indicates that previous X-ray data did not provide sufficiently constrained evidence that the larger stress per motor in phase 1 makes a significant contribution to the Δz-dependent mechanism of motor recruitment.

On the other hand, the present results also have some degree of uncertainty in the opposite demonstration that e_m/e_{m0} *versus* Δz relations in phase 1 and 2 are not different. The data comparison in Fig. 7*C* shows, in fact, that all phase 1 data lie within the 95% prediction bands of the phase 2 relation but, in the range of $\Delta z < 2$ nm, the phase 1 data are consistently above the phase 2 relation. Thus, even if the difference has not been demonstrated, the alternative conclusion that the two sets of data belong to a unique relation has also not been demonstrated within the limits of the present investigation. Consequently we have fitted the phase 2 data separately.

The average force per motor is reduced by motor recruitment

The stretch-induced recruitment of new motors affects the force response while, in turn, the force per motor reduces (Brunello *et al.* 2007), even if in the short time window considered the force per motor is spread over quite a large range. Taking motor recruitment into account, at the end of the stretch the average force per motor, relative to the isometric force, is $(T_1^*/T_0) \times (e_{m0}/e_m)$, where T_1^* is the average of T_1 for two consecutive ΔL values. As shown in Fig. 9 (open circles), the force per motor rises with the stretch size in the range of stretches used, attaining twice the T_0 value for the largest stretch. At 2 ms after the stretch, when force has dropped to T_2, the average force per motor relative to the T_0 value (calculated as $(T_2/T_0) \times (e_{m0}/e_m)$) is ∼1, independent of the stretch size (Fig. 9, filled circles). This indicates that, in the 2 ms following the stretch, further motor attachment is so effective that it brings the average force per motor back to its isometric value. For $\Delta L > 7$ nm hs^{-1}, corresponding to a $\Delta z > 5$ nm at 2 ms, the force per motor shows a small increase, consistent with the finding that the recruitment of new motors approaches saturation (Fig. 6*C* and *D*). All the above analysis relies on the assumption that, within the range of steps used (2–8 nm hs^{-1}), motor detachment, if any, is so small that it does not affect the conclusions. Actually, at least for phase 1, this must be valid also for larger stretches, as made evident by the data in Fig. 9 of Lombardi & Piazzesi (1990), where the T_1 value attained for a 12 nm hs^{-1} stretch was 4.2 T_0. This conclusion appears to nullify the assumption that it is possible to measure the rupture force of the actomyosin bond using the response of an actively contracting fibre to stretches of different speed (Colombini *et al.* 2007). During the stretch, as shown here, new motors are rapidly recruited; consequently, the conditions for applying Bell's equation (Bell, 1978; Seifert, 2000) are not satisfied.

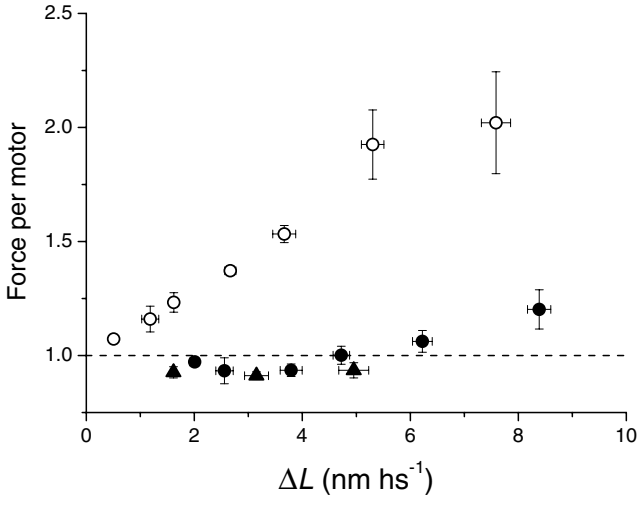

Figure 9. Average force per motor after the stretch
Average force per myosin motor relative to the isometric value (dashed line) at the end of the stretch (open circles) and at 2 ms following the stretch (filled circles and triangles) against the stretch size, calculated using the respective e_m/e_{m0} value from relations in Fig. 7*B*.

Mechanical evidence for recruitment of partner motors

Previous X-ray work suggested the idea that the myosin motors that rapidly attach on stretch are the partners of the motors already attached in isometric contraction. Further support for this idea is given by the finding, described in detail in this work, that the maximum stiffness of the motor array (e_m/e_{m0}) approaches twice the isometric value (Fig. 6*D*), as expected following the attachment to actin of all the second motor domains of the molecules with the first motor domain already attached. However, the level of saturation may be influenced by motor detachment that becomes very fast at a critical degree of strain (Colombini *et al.* 2007). This would produce an underestimate of the maximum number of recruited motors and explain why the maximum value of e_m/e_{m0} estimated by the sigmoidal fit in Fig. 6*D* does not attain a value of 2. Alternatively, a sharp rise in the detachment rate for $\Delta z > 6$ nm, followed by rapid reattachment (Lombardi & Piazzesi, 1990), could *per se* explain the saturation of e_m/e_{m0} at about 2, challenging the conclusion that the fast attachment concerns the partner motor domains. An estimate of how much rapid motor detachment–reattachment beyond a critical strain might affect the saturation process can be obtained from

experiments like that in Fig. 6*B*, by calculating the change in half-sarcomere stiffness and e_m/e_{m0} separately for the small test release (that implies subtracting a small amount of the strain generated by the conditioning stretch) and for the small test stretch (that implies increasing by a small amount the strain generated by the conditioning stretch). The results of this analysis are shown in Fig. 10. It can be seen that the relation obtained with the small test release (open triangles) and that obtained with the small test stretch (open squares) almost superpose on the filled circles from Fig. 6*D*, except for the conditioning stretch of 8 nm hs^{-1}: in this case, the point for the test stretch lies below and that for the test release lies above the point estimated as in Fig. 6*D*. Thus, at 2 ms following a stretch of 8 nm hs^{-1}, when the distortion of the attached motors attains ~6 nm, there is a significant influence of the direction of the test step on the estimate of the number of motors recruited by the conditioning stretch. The small test stretch (~1 nm hs^{-1}) provides an e_m/e_{m0} value of 1.7 (slightly smaller than the value obtained with the conditioning stretch of 6 nm hs^{-1}): this can be explained by considering that further motor attachment is balanced by the sharp rise in motor detachment. The maximum value of e_m/e_{m0} for small test releases, estimated by the sigmoidal equation fitted to the open triangles (dashed line) is 2.25 ± 0.18, *ca* 20% larger than the maximum value estimated by the sigmoidal equation fitted to either the filled circles (continuous line) or all stiffness data in Fig. 6*D* (filled circles and triangles), but not significantly different from 2 ($P > 0.1$). Thus, a ratio higher than 2 cannot be absolutely excluded. This implies that, within the 2 ms explored by the present experiments, it cannot be established whether a stretch is able to induce only attachment of the partner motor domains from the myosin molecules with the first motor domain already attached or also attachment of motor domains from detached myosin molecules. Moreover, the above analysis provides evidence that stretch-induced detachment of myosin motors takes place in the millisecond time scale at motor distortions above 6 nm.

Kinetics and mechanism of motor attachment by stretch

Considering that the duration of the stretch is 100 μs and that there is no evidence of a lag in the attainment of the equilibrium value by the stiffness–Δz relation (Fig. 7*C*), the process of recruitment must have a rise time (t_r) at least three times shorter than the rise time of the stretch (Milman & Taub, 1965), that is $\leq$30 μs. Assuming the process is exponential, the rate constant of the attachment of new motors, r ($=2.2/t_r$), must be $\geq 7.5 \times 10^4$ s^{-1}, that is in the range of values for the attachment–detachment of weakly binding myosin cross-bridges (Schoenberg *et al.* 1988).

The finding that, 2 ms after a stretch of 2–8 nm hs^{-1} superposed on an isometrically contracting fibre, the increase in stiffness of the array of motors saturates at twice the isometric value indicates that, within these 2 ms, the response to a stretch is related to the fraction of myosin molecules attached to actin in isometric contraction. According to a wide range of evidence from X-ray diffraction experiments (Juanhuix *et al.* 2001; Piazzesi *et al.* 2002, 2007; Reconditi *et al.* 2004; Huxley *et al.* 2006*b*; Brunello *et al.* 2007), the light chain domain (the lever arm) of the partner detached head relative to that of the attached head is tilted by only 10–15 deg toward the centre of the sarcomere in isometric contraction. This would make it difficult for the partner head to attach stereospecifically to the nearest available actin towards the centre of the sarcomere. However, within the 2 ms following a 2–8 nm hs^{-1} stretch, the local Z-ward shift by 1–5 nm of the actin filament with respect to the myosin filament would relieve this steric constraint, allowing attachment of the partner head to the next actin monomer towards the centre of the sarcomere. The sigmoidal fit to the relation in Fig. 6*D* indicates that the probability of attachment is greatest for a Δz of 2–3 nm. This can be explained by the concurrence of two events: (i) the first motor domain has to move sufficiently away from the partner motor toward the Z-line and (ii) the next M-ward actin monomer has shifted towards the catalytic domain of the partner motor. This mechanism agrees with the finding that the order of the reaction is close to 2.

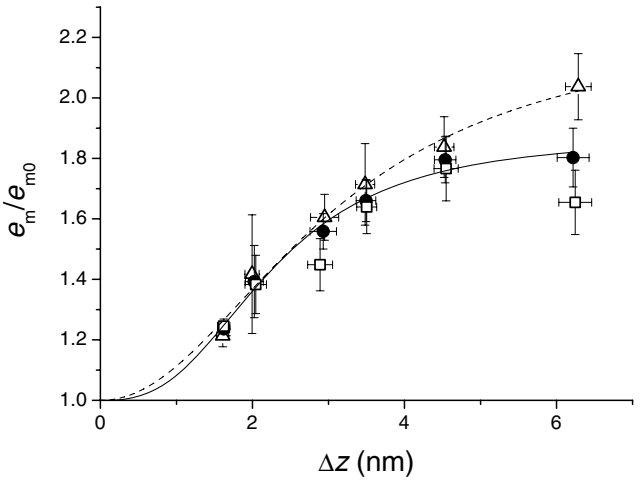

Figure 10. Comparison between stiffness of the motor array estimated with step stretches (open squares) and step releases (open triangles)
Filled circles are the same as in Fig. 6*D*. The lines are the sigmoidal fits (same equation as in Fig. 6*D*) to filled circles (continuous line, $A = 0.87 \pm 0.05$, $k = 2.27 \pm 0.15$ nm and $n = 2.75 \pm 0.45$) and open triangles (dashed line, $A = 1.25 \pm 0.18$, $k = 3.06 \pm 0.52$ nm and $n = 2.07 \pm 0.43$).

The formation of the proper interface between the motor domain and the actin should explain the $7.5 \times 10^4\ s^{-1}$ rate of attachment, and is similar to the kinetics of detachment–attachment of weakly binding myosin cross-bridges. In contrast with weakly binding kinetics, in this case the detachment rate must be much smaller since the motors remain strongly bound to actin. The shift of the equilibrium fully in favour of the bound state can be explained by the fact that, during both the stretch and the force recovery following the stretch, the reaction occurs while the actin site is not stationary but is moving away from the centre of the sarcomere. This explains how the energy of the stretch on the sarcomere is transferred to the level of the single actin–myosin interaction. Thus, rapid attachment of new motors is based on the dimeric structure of the myosin that, depending on the Z-ward movement of the first motor domain, allows the rapid interaction between the second motor domain and the actin and the consequent capture of the energy of the actin movement that stabilises the bond. This seems to be a general mechanism for muscle response to stretch, not specific to skeletal muscle, as shown by X-ray diffraction experiments on insect flight muscle (Bekyarova *et al.* 2008) and by the strain dependence of rate of attachment of myosin VI to actin (Iwaki *et al.* 2009).

Reflections on the response of active muscle to steady lengthening

During the force response to steady lengthening under conditions that preserve the sarcomere length homogeneity, the half-sarcomere stiffness and thus the number of attached motors remain high independently of the increase in the lengthening velocity and rate of motor detachment (Lombardi & Piazzesi, 1990).

This was explained with an actin–myosin interaction cycle that is different from that responsible for generation of force and shortening by muscle: during steady lengthening myosin motors attach very quickly to actin and, beyond a critical value of distortion, very quickly detach without commitment to ATP hydrolysis. We suggest that the mechanism postulated here for the rapid formation of a strong bond, once the correct myosin interface is presented to an actin monomer sliding in the Z-ward direction, is a mechanism that involves not only the second motor domains of the attached myosin molecules following a stretch, but also the motor domains of detached molecules during steady lengthening. This is therefore a general mechanism that is able to explain the high resistance of active muscle to stretch for both transient and steady-state responses. This mechanism would also explain why the force enhancement in response to steady lengthening is inversely related to the level of force developed during the preceding isometric contraction (Stienen *et al.* 1992). Independently of the factor (inorganic phosphate (Stienen *et al.* 1992) or vanadate (Getz *et al.* 1998)) that inhibits the formation of force generating actin–myosin interactions and maintains a larger fraction of motors in the weakly binding state during isometric contraction, during steady lengthening the same number of motors and thus the same steady force should be attained because, for any actin–myosin encounter, there will be a rapid shift from a weak to a strong interaction.

References

Bekyarova TI, Reedy MC, Baumann BA, Tregear RT, Ward A, Krzic U, Prince KM, Perz-Edwards RJ, Reconditi M, Gore D, Irving TC & Reedy MK (2008). Reverse actin sliding triggers strong myosin binding that moves tropomyosin. *Proc Natl Acad Sci U S A* **105**, 10372–10377.

Bell GI (1978). Models for the specific adhesion of cells to cells. *Science* **200**, 618–627.

Bordas J, Svensson A, Rothery M, Lowy J, Diakun GP & Boesecke P (1999). Extensibility and symmetry of actin filaments in contracting muscles. *Biophys J* **77**, 3197–3207.

Bressler BH, Dusik LA & Menard MR (1988). Tension responses of frog skeletal muscle fibres to rapid shortening and lengthening steps. *J Physiol* **397**, 631–641.

Brunello E, Bianco P, Piazzesi G, Linari M, Reconditi M, Panine P, Narayanan T, Helsby WI, Irving M & Lombardi V (2006). Structural changes in the myosin filament and cross-bridges during active force development in single intact frog muscle fibres: stiffness and X-ray diffraction measurements. *J Physiol* **577**, 971–984.

Brunello E, Reconditi M, Elangovan R, Linari M, Sun YB, Narayanan T, Panine P, Piazzesi G, Irving M & Lombardi V (2007). Skeletal muscle resists stretch by rapid binding of the second motor domain of myosin to actin. *Proc Natl Acad Sci U S A* **104**, 20114–20119.

Colombini B, Bagni MA, Romano G & Cecchi G (2007). Characterization of actomyosin bond properties in intact skeletal muscle by force spectroscopy. *Proc Natl Acad Sci U S A* **104**, 9284–9289.

Colomo F, Lombardi V & Piazzesi G (1987). Stiffness during tension recovery after a step stretch applied to tetanized frog muscle fibres during steady lengthening. *J Physiol* **390**, 148P.

Conibear PB & Geeves MA (1998). Cooperativity between the two heads of rabbit skeletal muscle heavy meromyosin in binding to actin. *Biophys J* **75**, 926–937.

Cooke R & Franks K (1980). All myosin heads form bonds with actin in rigor rabbit skeletal muscle. *Biochemistry* **19**, 2265–2269.

Curtin NA & Davies RE (1973). Chemical and mechanical changes during stretching of activated frog skeletal muscle. *Cold Spring Harbor Symp Quant Biol* **37**, 619–626.

Davis JS & Rodgers ME (1995). Force generation and temperature-jump and length-jump tension transients in muscle fibres. *Biophys J* **68**, 2032–2040.

Davis JS & Rodgers ME (1996). The two myosin heads function sequentially in non-tension and tension generating modes during isometric contraction. *Biophys J* **70**, A126.

Decostre V, Bianco P, Lombardi V & Piazzesi G (2005). Effect of temperature on the working stroke of muscle myosin. *Proc Natl Acad Sci U S A* **102**, 13927–13932.

Dobbie I, Linari M, Piazzesi G, Reconditi M, Koubassova N, Ferenczi MA, Lombardi V & Irving M (1998). Elastic bending and active tilting of myosin heads during muscle contraction. *Nature* **396**, 383–387.

Drummond GB (2009). Reporting ethical matters in *The Journal of Physiology*: standards and advice. *J Physiol* **587**, 713–719.

Edman KA (1966). The relation between sarcomere length and active tension in isolated semitendinosus fibres of the frog. *J Physiol* **183**, 407–417.

Edman KA (2009). Non-linear myofilament elasticity in frog intact muscle fibres. *J Exp Biol* **212**, 1115–1119.

Edman KA, Elzinga G & Noble MI (1982). Residual force enhancement after stretch of contracting frog single muscle fibres. *J Gen Physiol* **80**, 769–784.

Edman KA & Tsuchiya T (1996). Strain of passive elements during force enhancement by stretch in frog muscle fibres. *J Physiol* **490**, 191–205.

Fajer PG, Fajer EA, Brunsvold NJ & Thomas DD (1988). Effects of AMPPNP on the orientation and rotational dynamics of spin-labelled muscle cross-bridges. *Biophys J* **53**, 513–524.

Ford LE, Huxley AF & Simmons RM (1977). Tension responses to sudden length change in stimulated frog muscle fibres near slack length. *J Physiol* **269**, 441–515.

Ford LE, Huxley AF & Simmons RM (1981). The relation between stiffness and filament overlap in stimulated frog muscle fibres. *J Physiol* **311**, 219–249.

Getz EB, Cooke R & Lehman SL (1998). Phase transition in force during ramp stretches of skeletal muscle. *Biophys J* **75**, 2971–2983.

Gordon AM, Huxley AF & Julian FJ (1966). The variation in isometric tension with sarcomere length in vertebrate muscle fibres. *J Physiol* **184**, 170–192.

Herzog W & Leonard TR (2002). Force enhancement following stretching of skeletal muscle: a new mechanism. *J Exp Biol* **205**, 1275–1283.

Higuchi H, Yanagida T & Goldman YE (1995). Compliance of thin filaments in skinned fibres of rabbit skeletal muscle. *Biophys J* **69**, 1000–1010.

Huxley AF & Lombardi V (1980). A sensitive force transducer with resonant frequency 50 kHz. *J Physiol* **305**, 15*P*–16*P*.

Huxley AF, Lombardi V & Peachey LD (1981). A system for fast recording of longitudinal displacement of a striated muscle fibre. *J Physiol* **317**, 12*P*–13*P*.

Huxley AF & Tideswell S (1997). Rapid regeneration of power stroke in contracting muscle by attachment of second myosin head. *J Muscle Res Cell Motil* **18**, 111–114.

Huxley HE & Brown W (1967). The low-angle x-ray diagram of vertebrate striated muscle and its behaviour during contraction and rigor. *J Mol Biol* **30**, 383–434.

Huxley HE, Reconditi M, Stewart A & Irving T (2006*a*). X-ray interference studies of crossbridge action in muscle contraction: evidence from quick releases. *J Mol Biol* **363**, 743–761.

Huxley HE, Reconditi M, Stewart A & Irving T (2006*b*). X-ray interference studies of crossbridge action in muscle contraction: evidence from muscles during steady shortening. *J Mol Biol* **363**, 762–772.

Huxley HE, Stewart A, Sosa H & Irving T (1994). X-ray diffraction measurements of the extensibility of actin and myosin filaments in contracting muscle. *Biophys J* **67**, 2411–2421.

Infante AA, Klaupiks D & Davies RE (1964). Adenosine triphosphate: changes in muscles doing negative work. *Science* **144**, 1577–1578.

Iwaki M, Iwane AH, Shimokawa T, Cooke R & Yanagida T (2009). Brownian search-and-catch mechanism for myosin-VI steps. *Nat Chem Biol* **5**, 403–405.

Juanhuix J, Bordas J, Campmany J, Svensson A, Bassford ML & Narayanan T (2001). Axial disposition of myosin heads in isometrically contracting muscles. *Biophys J* **80**, 1429–1441.

Katz B (1939). The relation between force and speed in muscular contraction. *J Physiol* **96**, 45–64.

Knupp C, Offer G, Ranatunga KW & Squire JM (2009). Probing muscle myosin motor action: x-ray (m3 and m6) interference measurements report motor domain not lever arm movement. *J Mol Biol* **390**, 168–181.

Linari M, Brunello E, Reconditi M, Sun YB, Panine P, Narayanan T, Piazzesi G, Lombardi V & Irving M (2005). The structural basis of the increase in isometric force production with temperature in frog skeletal muscle. *J Physiol* **567**, 459–469.

Linari M, Caremani M, Piperio C, Brandt P & Lombardi V (2007). Stiffness and fraction of Myosin motors responsible for active force in permeabilized muscle fibres from rabbit psoas. *Biophys J* **92**, 2476–2490.

Linari M, Lucii L, Reconditi M, Casoni ME, Amenitsch H, Bernstorff S, Piazzesi G & Lombardi V (2000*a*). A combined mechanical and X-ray diffraction study of stretch potentiation in single frog muscle fibres. *J Physiol* **526**, 589–596.

Linari M, Piazzesi G, Dobbie I, Koubassova N, Reconditi M, Narayanan T, Diat O, Irving M & Lombardi V (2000*b*). Interference fine structure and sarcomere length dependence of the axial X-ray pattern from active single muscle fibres. *Proc Natl Acad Sci U S A* **97**, 7226–7231.

Linari M, Piazzesi G & Lombardi V (2009). The effect of myofilament compliance on kinetics of force generation by myosin motors in muscle. *Biophys J* **96**, 583–592.

Linari M, Woledge RC & Curtin NA (2003). Energy storage during stretch of active single fibres from frog skeletal muscle. *J Physiol* **548**, 461–474.

Lombardi V & Piazzesi G (1990). The contractile response during steady lengthening of stimulated frog muscle fibres. *J Physiol* **431**, 141–171.

Lombardi V, Piazzesi G & Linari M (1992). Rapid regeneration of the actin-myosin power stroke in contracting muscle. *Nature* **355**, 638–641.

Lovell SJ, Knight PJ & Harrington WF (1981). Fraction of myosin heads bound to thin filaments in rigor fibrils from insect flight and vertebrate muscles. *Nature* **293**, 664–666.

Mantovani M, Cavagna GA & Heglund NC (1999). Effect of stretching on undamped elasticity in muscle fibres from *Rana temporaria*. *J Muscle Res Cell Motil* **20**, 33–43.

Milman J & Taub H (1965). *Pulse, Digital and Switching Waveforms*, pp. 47–48. McGraw-Hill, New York.

Morgan DL (1990). New insights into the behaviour of muscle during active lengthening. *Biophys J* **57**, 209–221.

Morgan DL (1994). An explanation for residual increased tension in striated muscle after stretch during contraction. *Exp Physiol* **79**, 831–838.

Noble MI (1992). Enhancement of mechanical performance of striated muscle by stretch during contraction. *Exp Physiol* **77**, 539–552.

Pate E & Cooke R (1988). Energetics of the actomyosin bond in the filament array of muscle fibres. *Biophys J* **53**, 561–573.

Piazzesi G, Linari M, Reconditi M, Vanzi F & Lombardi V (1997). Cross-bridge detachment and attachment following a step stretch imposed on active single frog muscle fibres. *J Physiol* **498**, 3–15.

Piazzesi G, Reconditi M, Koubassova N, Decostre V, Linari M, Lucii L & Lombardi V (2003). Temperature dependence of the force-generating process in single fibres from frog skeletal muscle. *J Physiol* **549**, 93–106.

Piazzesi G, Reconditi M, Linari M, Lucii L, Bianco P, Brunello E, Decostre V, Stewart A, Gore DB, Irving TC, Irving M & Lombardi V (2007). Skeletal muscle performance determined by modulation of number of Myosin motors rather than motor force or stroke size. *Cell* **131**, 784–795.

Piazzesi G, Reconditi M, Linari M, Lucii L, Sun YB, Narayanan T, Boesecke P, Lombardi V & Irving M (2002). Mechanism of force generation by myosin heads in skeletal muscle. *Nature* **415**, 659–662.

Reconditi M (2010). There is no experimental evidence for non-linear myofilament elasticity in skeletal muscle. *J Exp Biol* **in press**.

Reconditi M, Linari M, Lucii L, Stewart A, Sun YB, Boesecke P, Narayanan T, Fischetti RF, Irving T, Piazzesi G, Irving M & Lombardi V (2004). The myosin motor in muscle generates a smaller and slower working stroke at higher load. *Nature* **428**, 578–581.

Schoenberg M, Sugi H & Pollack GH (1988). The kinetics of weakly-and strongly-binding crossbridges: implications for contraction and relaxation. In *Molecular Mechanism of Muscle Contraction*, pp. 189. Plenum Press.

Seifert U (2000). Rupture of multiple parallel molecular bonds under dynamic loading. *Phys Rev Lett* **84**, 2750–2753.

Smith DA, Geeves MA, Sleep J & Mijailovich SM (2008). Towards a unified theory of muscle contraction. I: foundations. *Ann Biomed Eng* **36**, 1624–1640.

Stienen GJ, Versteeg PG, Papp Z & Elzinga G (1992). Mechanical properties of skinned rabbit psoas and soleus muscle fibres during lengthening: effects of phosphate and Ca^{2+}. *J Physiol* **451**, 503–523.

Sugi H & Tsuchiya T (1988). Stiffness changes during enhancement and deficit of isometric force by slow length changes in frog skeletal muscle fibres. *J Physiol* **407**, 215–229.

Thomas DD & Cooke R (1980). Orientation of spin-labelled myosin heads in glycerinated muscle fibres. *Biophys J* **32**, 891–906.

Tsaturyan AK, Koubassova N, Ferenczi MA, Narayanan T, Roessle M & Bershitsky SY (2005). Strong binding of myosin heads stretches and twists the actin helix. *Biophys J* **88**, 1902–1910.

Tyska MJ, Dupuis DE, Guilford WH, Patlak JB, Waller GS, Trybus KM, Warshaw DM & Lowey S (1999). Two heads of myosin are better than one for generating force and motion. *Proc Natl Acad Sci U S A* **96**, 4402–4407.

Wakabayashi K, Sugimoto Y, Tanaka H, Ueno Y, Takezawa Y & Amemiya Y (1994). X-ray diffraction evidence for the extensibility of actin and myosin filaments during muscle contraction. *Biophys J* **67**, 2422–2435.

Author contributions

All authors contributed to the conception and design of the experiments. L.F. made the main contributions to data analysis. All authors contributed to data interpretation, drafting and critical revision of the article for important intellectual content. All authors have approved the final version to be published. All experiments were performed at the Laboratory of Physiology, Department of Evolutionary Biology, Florence (Italy).

Acknowledgements

We thank M. Dolfi for mechanical and electronics support, Professor Ed Taylor for discussion and suggestions on the preliminary version of the paper and Professor Malcolm Irving for reading the manuscript. This work was supported by Ministero dell'Istruzione, dell'Università e della Ricerca (Italy) and National Institutes of Health R01 AR049033 (USA).